This article has been accepted for publication in IEEE Wireless Communications Letters. This is the author's version which has not been fully edited and content may change prior to final publication. Citation information: DOI 10.1109/LWC.2025.3588223

Dynamic Channel Modeling of Fluid Antenna Systems in UAV Communications

Hao Jiang, *Member, IEEE,* Wangqi Shi, Zhen Chen, *Senior Member, IEEE,* Zaichen Zhang, *Senior Member, IEEE,* Kai-Kit Wong, *Fellow, IEEE,* and Hyundung Shin, *Fellow, IEEE*

***Abstract*—As an emerging wireless communication technology, fluid antenna system (FAS) shows great potential for its reconfigurable radiation characteristics that can benefit air-to-ground (A2G) communications. In this letter, we propose a novel dynamic port-reconfigurable channel model for FAS-assisted unmanned aerial vehicle (UAV)-to-ground user (GU) A2G communications. Unlike conventional static antenna models, the proposed framework integrates the unique ability of FAS to dynamically activate and reconfigure antenna ports, enabling accurate simulation of FAS behaviors across diverse communication scenarios. Crucial performance indicators, such as modeling accuracy and channel capacity, are derived and investigated, revealing that the number of active ports and port spacing significantly impact both metrics. The dynamic characteristics of UAV is also shown to significantly affect the channel capacities, emphasizing the requirements for adaptive FAS configuration in A2G scenarios. These findings offer valuable insights for the design and analysis of FAS, particularly in dynamic environments like UAV communications.**

***Index Terms*—Channel capacity, channel modelling, fluid antenna, MIMO, movable antenna, modeling accuracy.**

I. Introduction

THE ADVENT of the sixth-generation (6G) indicates a revolutionary leap in wireless communication, characterized by groundbreaking data transmission speeds, extremely low latency and ultra-reliable connectivity [1], [2], [3]. To achieve these requirements, researchers are actively exploring innovative technologies to push the boundaries of current wireless systems. Leading these innovation efforts is multiple-input multiple-output (MIMO) antenna system that has been the core technology, showing significant advantages in spectral efficiency, channel capacity and link reliability [4], [5].

The essence of MIMO lies in utilizing multiple antennas to create multiple propagation paths for enhancing the capacity of communication systems from spatial diversity [6]. The practice is that the spacing between adjacent antennas should be at least half a wavelength for MIMO to be effective because of mutual coupling and spatial correlation that could limit diversity. The problem of this rule, however, is that the number of antennas at a terminal, base station (BS) or ground user (GU), will be constrained by the available space. Additionally, the capability of MIMO is dictated by the number of radio-frequency (RF) chains. But more RF chains means higher cost. In summary, these factors put the scalability of MIMO in doubt.

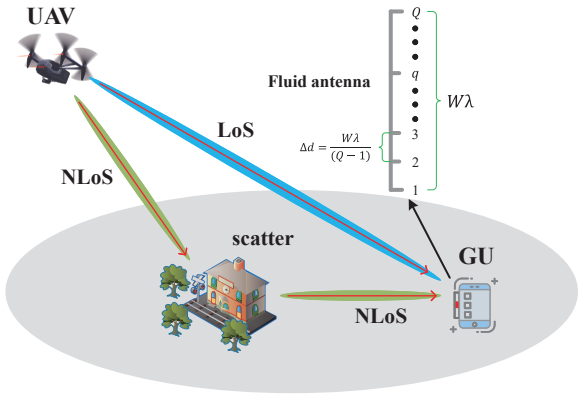

Fig. 1. A FAS-assisted UAV-to-GU wireless communication scenario.

Motivated by this, fluid antenna system (FAS) has recently emerged as a technology that can utilize the spatial diversity in fine space for enhancing the performance of wireless systems [7]. FAS was first introduced by Wong *et al.* in [8], [9], [10]. FAS is a broad concept that advocates the use of shape and position reconfigurable antenna technologies to empower the physical layer for performance enhancement. A recent article gives the theoretical foundation of what fluid antenna entails from the electromagnetic perspective [11]. Some implementation prototypes for FAS were reported in [12].

With increasing interest in FAS recently, efforts have been made to develop mathematically tractable models for characterizing the performance of FAS under rich scattering environments [13], [14]. A great deal of results on the diversity gain of FAS can be found in, e.g., [15] and [16]. The work in [17] further investigated the diversity and multiplexing trade-off of the MIMO channel with multiple fluid antennas at both ends while [18] also studied FAS with continuous positioning.

FAS also uncovers exciting new opportunities for multiple access. Specifically, it can take advantage of the position where the interference goes into a deep fade so that the desired signal can be received without interference. This has resulted in the several approaches of fluid antenna multiple access (FAMA), classified as fast [19], [20], slow [21], [22], and coded [23] with varying interference rejection capability. The

This work was supported by the National Natural Science Foundation of China (NSFC) projects (No. 62471238 and 62371197) and Jiangxi Province Science and Technology development Programme (No. 20242BCC32016). (*Corresponding author: Zhen Chen*).

H. Jiang is with the School of Artificial Intelligence, Nanjing University of Information Science and Technology, Nanjing 210044, China, and also with the National Mobile Communications Research Laboratory, Southeast University, Nanjing 210096, China, and also with the School of Information Engineering, Jiangxi Provincial Key Laboratory of Advanced Signal Processing and Intelligent Communications, Nanchang University, Nanchang 330031, China (e-mail: jianghao@nuist.edu.cn).

Z. Chen is with the College of Cyber Security, Jinan Universiy (e-mail: chenz.scut@gmail.com).

W. Shi and Z. Zhang are with the National Mobile Communications Research Laboratory, Southeast University, Nanjing 210096, China (e-mails: zczhang, shiwangqi@seu.edu.cn).

K. K. Wong is with the Department of Electronic and Electrical Engineering, University College London, WC1E 7JE London, United Kingdom, and also with the Department of Electronic Engineering, Kyung Hee University, Yongin-si, Gyeonggi-do 17104, Republic of Korea. (e-mail: kaikit.wong@ucl.ac.uk).

H. Shin is with the Department of Electronics and Information Convergence Engineering, Kyung Hee University, Yongin-si, Gyeonggi-do 17104, Republic of Korea (e-mail: hshin@khu.ac.kr).

This article has been accepted for publication in IEEE Wireless Communications Letters. This is the author's version which has not been fully edited and content may change prior to final publication. Citation information: DOI 10.1109/LWC.2025.3588223

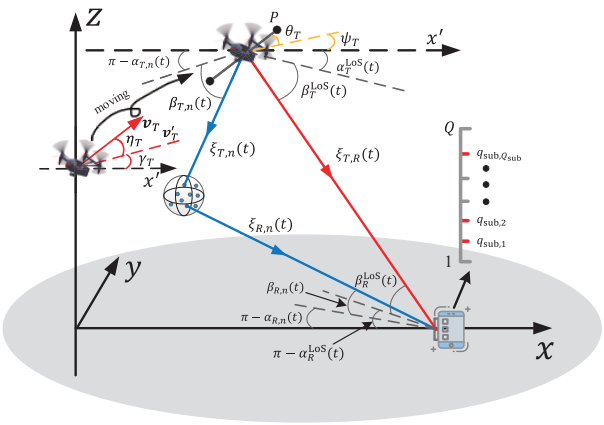

Fig. 2. The proposed FAS-assisted UAV channel model.

studies in [24] and [25] have introduced FAS technology into the multiple access for A2G communication, proving that the FAS is superior to the traditional antenna system. Moreover, opportunistic scheduling has been synergized with FAMA to serve more users [26]. There have also been active researches to devise channel estimation methods for FAS [27], [28]. Recent results have also considered FAS and reconfigurable intelligent surface (RIS) together [29], [30].

Despite the surge of efforts on FAS in recent years, channel modeling for FAS is still not sufficiently understood. In fact, existing efforts tend to focus on the cellular setup and those models would not be suitable for other emerging applications, such as air-to-ground (A2G) communications. Motivated by this, in this letter, our aim is to develop a general FAS-assisted A2G channel model which can adapt to various conditions in FAS communication by adjusting key parameters. It is worth mentioning that channel modeling in FAS communication systems differs significantly from that without FAS. Specifically, all modeling steps for FAS incorporate its dynamic characteristics, imparting new features to the channel model. Furthermore, this letter not only provides a detailed analysis of the model construction process but also investigates the modeling errors and channel capacity, revealing the impact of different FAS designs on system performance.

II. System Model

As shown in Figs. 1 and 2, we propose a three-dimensional (3D) channel model for unmanned aerial vehicle (UAV)-to-GU communications in FAS, in which the GU has a linear FAS with a length of $W\lambda$ and Q ports with λ being the carrier wavelength. It is worth mentioning that Fig. 1 primarily serves to depict the scenario and the link composition of the proposed channel model, whereas Fig. 2 is dedicated to detailing the parameter annotation of the model. Then the distance between the adjacent ports in FAS can be expressed as

$$\Delta d = \frac{W\lambda}{(Q-1)}. \tag{1}$$

The UAV is equipped with P omni-directional uniform linear array (ULA) antennas, and the azimuth and elevation orientation angles of the ULA are denoted by ψ_T and θ_T, respectively. Also, the azimuth and elevation orientation angles of the FAS are denoted by ψ_R and θ_R, respectively. The UAV keeps moving with a speed of v_T, and the azimuth and elevation angles in the direction of the motion are γ_T and η_T, respectively. In the proposed 3D coordinate system, the projection of midpoint of the UAV on the ground is defined as the coordinate origin, and the direction pointing to the GU is the positive direction of the x-axis; the z axis goes straight up and y-axis follows the right-hand rule. Define H_0 and D_0 as the initial altitude of the UAV and the distance from the origin to the GU, respectively. The time-varying position of the UAV can be expressed as

$$\mathbf{d}_T(t) = v_T t \begin{bmatrix} \cos\eta_T \cos\gamma_T \\ \cos\eta_T \sin\gamma_T \\ \sin\eta_T \end{bmatrix}, \tag{2}$$

where t denotes the motion time, and the other parameters are specified in Fig. 2. The distance vector from the p-th antenna to the midpoint of ULA at the UAV is given by

$$\mathbf{d}_{T,p} = k_p \delta_T \begin{bmatrix} \cos\theta_T \cos\psi_T \\ \cos\theta_T \sin\psi_T \\ \sin\theta_T \end{bmatrix}, \tag{3}$$

with $k_p = (P-2p+1)/2$, which service to simplify the formula, and thus the position of the p-th element in ULA can be expressed as

$$\mathbf{d}_p(t) = \begin{bmatrix} d_{p,x}(t) \\ d_{p,y}(t) \\ d_{p,z}(t) \end{bmatrix} = \mathbf{d}_{T,p} - \mathbf{d}_T(t). \tag{4}$$

At the GU, its position is defined as $\mathbf{d}_R = [D_0, 0, 0]^{\mathrm{T}}$.

The signal transmitted from the UAV will go through two types of propagation before reaching the GU. They are line-of-sight (LoS) components, where the signal from the UAV goes straight to the GU, and non-LoS (NLoS) components, where the signal undergoes scattering by the cluster before arriving at the GU. Assuming that these two propagation components are independent of each other, we can represent the complete channel matrix for the proposed channel model as

$$\mathbf{H}_{\text{FAS}}(t,\tau) = \mathbf{H}_{\text{FAS}}^{\text{LoS}}(t,\tau) + \mathbf{H}_{\text{FAS}}^{\text{NLoS}}(t,\tau), \tag{5}$$

where τ denotes the path delay, $\mathbf{H}_{\text{FAS}}^{\text{LoS}}(t,\tau)$ and $\mathbf{H}_{\text{FAS}}^{\text{NLoS}}(t,\tau)$ are the channel matrices for the LoS and NLoS propagation links. It is important to note that the dimension of $\mathbf{H}_{\text{FAS}}(t,\tau)$ is $Q_{\text{sub}} \times P$, with Q_{sub} standing for the number of active ports at the GU side, as shown in Fig. 2. In fact, Q_{sub} is a variable because in real fluid antenna communication scenario, one or multiple ports are activated for communication. In this letter, we introduce the general form of the channel matrix for FAS and employ Q_{sub} to signify the count of active ports. It is worth mentioning that the lowercase, boldface lowercase, uppercase letters, and boldface uppercase letters such as x, $\mathbf{x}$, X, and $\mathbf{X}$ stand for the scalars, vectors, sets, and matries, respectively. Therefore, the set of Q_{sub} can be expressed as

$$\mathrm{Q}_{\text{sub}} = \{q_{\text{sub},1}, q_{\text{sub},2}, \ldots, q_{\text{sub},Q_{\text{sub}}}\} \in \mathrm{Q}, \tag{6}$$

This article has been accepted for publication in IEEE Wireless Communications Letters. This is the author's version which has not been fully edited and content may change prior to final publication. Citation information: DOI 10.1109/LWC.2025.3588223

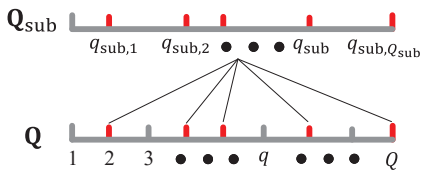

Fig. 3. The relationship between $\mathrm{Q}_{\mathrm{sub}}$ and Q.

where $\mathrm{Q} = 1, 2, \ldots, Q$ denotes the set of the ports at the GU side. The relationship between Q and $\mathrm{Q}_{\mathrm{sub}}$ is shown in Fig. 3, where the red port represents the active port.

Then the position of the q_{sub}-th ($q_{\mathrm{sub}} = 1, 2, \ldots, Q_{\mathrm{sub}}$) can be expressed as

$$\mathbf{d}_{q_{\mathrm{sub}}} = k_{q_{\mathrm{sub}}} \Delta d \begin{bmatrix} \cos\theta_R \cos\psi_R \\ \cos\theta_R \sin\psi_R \\ \sin\theta_R \end{bmatrix} - \begin{bmatrix} D_0 \\ 0 \\ 0 \end{bmatrix}, \quad (7)$$

where $k_{q_{\mathrm{sub}}} \Delta d$ denotes the distance between the q_{sub}-th port and the center point of FAS.

In (5), each element in $\mathbf{H}_{\mathrm{FAS}}(t, \tau)$ stands for the the complex channel impulse response (CIR) of the propagation link from the p-th element in ULA at the UAV side to the q_{sub}-th element in fluid antenna at the GU side, which can be expressed as

$$h_{p,q_{\mathrm{sub}}}(t,\tau) = \sqrt{\frac{K}{K+1}} h^{\mathrm{LoS}}_{p,q_{\mathrm{sub}}}(t)\delta\left(\tau - \tau^{\mathrm{LoS}}(t)\right) + \sqrt{\frac{1}{K+1}} h^{\mathrm{NLoS}}_{p,q_{\mathrm{sub}}}(t)\delta\left(\tau - \tau^{\mathrm{NLoS}}(t)\right), \quad (8)$$

where K is the Rician factor, which serves for the channel with the LoS link, $h^{\mathrm{LoS}}_{p,q_{\mathrm{sub}}}(t)$ and $h^{\mathrm{NLoS}}_{p,q_{\mathrm{sub}}}(t)$ are, respectively, the complex CIRs of the LoS and NLoS propagation link from the p-th element in ULA at the UAV side to the q_{sub}-th element in fluid antenna at the GU side. Furthermore, $\tau^{\mathrm{LoS}}(t)$ and $\tau^{\mathrm{NLoS}}(t)$ are, respectively, the path delay for the LoS and NLoS propagation links, which can be derived as the ratios of the lengths of the transmission path to the speed of light.

For the LoS component, the complex CIR from the p-th element in ULA at the UAV side to the q_{sub}-th element in fluid antenna at the GU side can be expressed as

$$\begin{aligned} h^{\mathrm{LoS}}_{p,q_{\mathrm{sub}}}(t) = {} & e^{-j\frac{2\pi}{\lambda}\xi_{T,R}(t)} \\ & \times e^{j\frac{2\pi}{\lambda}k_p\delta_T\cos\left(\alpha^{\mathrm{LoS}}_T(t)-\psi_T\right)\cos\beta^{\mathrm{LoS}}_T(t)\cos\theta_T} \\ & \times e^{j\frac{2\pi}{\lambda}k_p\delta_T\sin\beta^{\mathrm{LoS}}_T(t)\sin\theta_T} \\ & \times e^{j\frac{2\pi}{\lambda}k_{q_{\mathrm{sub}}}\cos\left(\alpha^{\mathrm{LoS}}_R(t)-\psi_R\right)\cos\beta^{\mathrm{LoS}}_R(t)\cos\theta_R} \\ & \times e^{j\frac{2\pi}{\lambda}k_{q_{\mathrm{sub}}}\Delta d\sin\beta^{\mathrm{LoS}}_R(t)\sin\theta_R} \\ & \times e^{j\frac{2\pi}{\lambda}v_T t\cos\left(\alpha^{\mathrm{LoS}}_T(t)-\gamma_T\right)\cos\beta^{\mathrm{LoS}}_T(t)\cos\eta_T} \\ & \times e^{j\frac{2\pi}{\lambda}v_T t\sin\beta^{\mathrm{LoS}}_T(t)\sin\eta_T}, \end{aligned} \quad (9)$$

where $\xi_{T,R}(t) = \|\mathbf{d}_R - \mathbf{d}_T(t)\|$ stands for the time-varying distance between the UAV and GU. The $\alpha^{\mathrm{LoS}}_T(t)$ and $\beta^{\mathrm{LoS}}_T(t)$ are respectively the time-varying angles of departure of the transmitted waves in the azimuth and vertical planes, which can be obtained by based on geometrical relationships. Furthermore, the last two lines represent the Doppler phase shift caused by the movement of the UAV, which is related to the speed, time and direction of motion.

For the NLoS component, the complex CIR from the p-th element in ULA at the UAV side to the q-th element in fluid antenna at the GU side can be expressed as

$$\begin{aligned} h^{\mathrm{NLoS}}_{p,q_{\mathrm{sub}}}(t) = {} & \sum_{\ell\in L}\sum_{n=1}^{\ell_N} e^{j\varphi_{\ell_n} - j\frac{2\pi}{\lambda}\left(\xi_{T,\ell_n}(t)+\xi_{R,\ell_n}\right)} \\ & \times e^{j\frac{2\pi}{\lambda}k_p\delta_T\cos\left(\alpha^{\mathrm{LoS}}_{T,\ell_n}(t)-\psi_T\right)\cos\beta^{\mathrm{LoS}}_{T,\ell_n}(t)\cos\theta_T} \\ & \times e^{j\frac{2\pi}{\lambda}k_p\delta_T\sin\beta^{\mathrm{LoS}}_{T,\ell_n}(t)\sin\theta_T} \\ & \times e^{j\frac{2\pi}{\lambda}k_{q_{\mathrm{sub}}}\Delta d\cos\left(\alpha^{\mathrm{LoS}}_{R,\ell_n}-\psi_R\right)\cos\beta^{\mathrm{LoS}}_{R,\ell_n}\cos\theta_R} \\ & \times e^{j\frac{2\pi}{\lambda}k_{q_{\mathrm{sub}}}\Delta d\sin\beta^{\mathrm{LoS}}_{R,\ell_n}\sin\theta_R} \\ & \times e^{j\frac{2\pi}{\lambda}v_T t\cos\left(\alpha^{\mathrm{LoS}}_{T,\ell_n}(t)-\gamma_T\right)\cos\beta^{\mathrm{LoS}}_{T,\ell_n}(t)\cos\eta_T} \\ & \times e^{j\frac{2\pi}{\lambda}v_T t\sin\beta^{\mathrm{LoS}}_{T,\ell_n}(t)\sin\eta_T}, \end{aligned} \quad (10)$$

where $\{\varphi_{\ell_n}\}_{n=1,2,\ldots,L_n}$ stands for the random phase, here we assume it is independent and follows a uniformly distribution of $[-\pi, \pi)$, that is, $\varphi_{\ell_n} \sim \mathrm{U}[-\pi, \pi)$. Besides, $\xi_{T,\ell_n}(t)$ and ξ_{R,ℓ_n} are the distances between UAV/GU and the n-th path in the ℓ-th cluster, respectively, which can be written as

$$\xi_{T,\ell_n}(t) = \|\mathbf{d}_{\ell_n} - \mathbf{d}_T(t)\|, \quad (11)$$

$$\xi_{R,\ell_n} = \|\mathbf{d}_{\ell_n} - \mathbf{d}_R\|, \quad (12)$$

where $\mathbf{d}_{\ell_n}$ represents the position of the n-th path in the ℓ-th cluster. Furthermore, $\alpha_{T,\ell_n}(t)$ and $\beta_{T,\ell_n}(t)$ are the time-varying angles of departure of the transmitted waves in the azimuth and vertical planes, respectively, which are derived by calculating the angle between the line connecting the q_{sub}-th element in the antenna array and the n-th path in the ℓ-th cluster and the x axis. Also, α_{R,ℓ_n} and β_{R,ℓ_n} are the angles of arrival of the waves in the azimuth and vertical planes, respectively. All the angles above can be derived based on geometrical relationships. In this letter, we introduce von Mises distribution to determine the position of each scatterer, which can be found from

$$f(\alpha) = \frac{e^{\kappa\cos(\alpha-\mu_\alpha)}}{2\pi I_0(\kappa)}, \quad (13)$$

where κ is the environment factor, μ_α is the mean of α, and $I_0(\cdot)$ represents a modified Bessel function of order 0. It is worth mentioning that the expressions for the CIR proposed in (9) and (10) are primarily referenced from [31] and [32]. These formulas accurately reflect the influence of relevant parameters of the channel model, including transmission paths, antenna spacing, transmit-receive angles, and UAV movement, on the characteristics of the proposed channel model.

III. Propagation Characteristics

For A2G wireless communication systems, modeling accuracy is an important evaluation target for channel models,

This article has been accepted for publication in IEEE Wireless Communications Letters. This is the author's version which has not been fully edited and content may change prior to final publication. Citation information: DOI 10.1109/LWC.2025.3588223

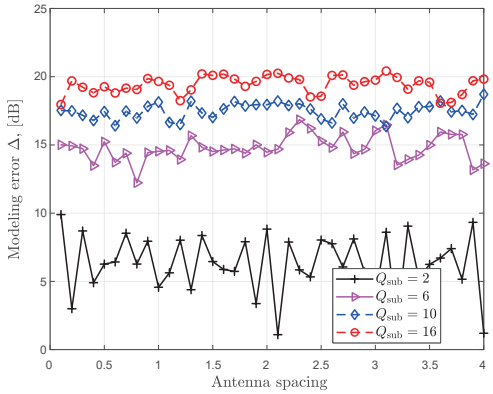

Fig. 4. Modeling error performance against the antenna spacing.

typically calculated based on the proposed model and a baseline model. Therefore, the normalized absolute error Δ can be found as

$$\Delta = 10\log_{10}\left\{\sum_{p=1}^{P}\sum_{q=1}^{Q}\frac{|h_{pq}(t,\tau) - h_{pq}^{\text{ULA}}(t,\tau)|}{|h_{pq}^{\text{ULA}}(t,\tau)|}\right\}, \quad (14)$$

where $h_{pq}^{\text{ULA}}(t,\tau)$ stands for the complex CIR of the baseline model. Here, we deploy a ULA in the same configuration at the GU side, while all other conditions remain unchanged. It is worth mentioning that the ULA has been widely discussed in the existing literature and has well channel characteristics. Therefore, we use the channel model corresponding to ULA as the benchmark model to measure the modeling accuracy of the proposed FAS channel model. Furthermore, if planar or other shaped FAS are considered, the MIMO channel model of the corresponding shape can also be used as the benchmark model.

Another metric for evaluating the performance of the FAS channel model is channel capacity, which is given by

$$C = \log_2\left(\det\left(\mathbf{I}_Q + \frac{\rho_{\text{SNR}}}{P}\overline{\mathbf{H}}(t,\tau)\overline{\mathbf{H}}^{\text{H}}(t,\tau)\right)\right), \quad (15)$$

with $\mathbf{I}_Q$ and ρ_{SNR} being the identity matrix of size $Q \times Q$ and the signal-to-noise ratio (SNR), respectively. Also, $\overline{\mathbf{H}}(t,\tau)$ denotes the normalized channel matrix, as referred to in [6] and [31], and it is omitted here due to space limitations.

IV. Results and Discussion

Here, numerical results of modeling accuracy and channel capacity of the FAS system are provided. The simulation parameters are set as follows: $f_c = 5$ GHz, $H_0 = 20$ m, $D_0 = 50$ m, $P = 4$, $Q = 20$, $\delta_T = \lambda/2$, $\psi_T = \pi/2$, $\theta_T = \pi/3$, $v_T = 3$ m/s, $\eta_T = \gamma_T = \pi/3$, and $t = 2$ s.

By using (14), Fig. 4 shows the modeling accuracy of the proposed FAS-assisted channel model against different number of active ports. It is worth noting that the symbol δ_R here denotes the spacing between adjacent antennas in ULA, whereas in FAS, it indicates the spacing between adjacent ports. The results demonstrate that the modeling error associated with the proposed FAS exhibits fluctuation with the increase of port spacing, which is caused by the different spacing of adjacent active ports in the FAS configuration. Another phenomenon is that when the number of active ports increases, the values of the error curve tend to rise, thereby leading to an increase in modeling error. This due to the fact that more active ports will enhance the mutual influence between adjacent ports.

Fig. 5 presents the performance comparison of the proposed FAS channel model. Fig. 5(a) illustrates the channel capacity of the proposed FAS channel model with respect to different numbers of active ports and different port spacings. It is worth mentioning that the alterations in W will indirectly result in changes to the port spacing. Consequently, we adjust the value of W to analyze the impact of the change of port spacing on the channel capacity. Analytical results reveal that the channel capacity of the proposed FAS channel model exhibits a positive correlation with the number of active ports, as expected. In addition, the channel capacity is also influenced by the port spacing, exhibiting noticeable variations under different spacing configurations. Specifically, larger port spacing leads to an increase in channel capacity. In combination with Fig. 4, it becomes evident that striving for higher channel capacity in practical FAS designs requires a trade-off with modeling accuracy, as increasing the number of active ports leads to both higher capacity and larger modeling errors.

Fig. 5(b) provides the channel capacity results of the proposed FAS-assisted channel model under various UAV motion states. The results reveal that dynamic characteristics of the UAV, such as its velocity and motion time, significantly influence the variations in channel capacity behavior, which is due to the influence brought by the Doppler effect and the time-varying channel. Specifically, when we increase the velocity of UAV, the channel capacity exhibits more noticeable fluctuations due to the variations in the channel model. Also, the motion time causes variations in channel conditions, which further impact the channel capacity. These findings underscore the significance of accounting for the dynamic characteristics of UAVs in the design of FAS-assisted UAV communication.

Fig. 5(c) shows the comparative analysis of channel capacities between the proposed FAS and conventional ULA systems. It is evident that FAS can achieve higher channel capacity than ULA, and more antenna ports in FAS enables greater spatial multiplexing gain, which directly contributes to enhanced data transmission capacity. Specifically, the architecture of FAS enables a denser spatial distribution of antenna elements, thereby overcoming the capacity limitations of ULA. Notably, the data reveals that when 67 percent of ports are activated, the channel capacity of FAS approaches that of ULA. This observation highlights the spatial efficiency of FAS. This is a distinct advantage that can reduce energy consumption and hardware complexity in practical deployments.

V. Conclusion

This letter has studied the channel modeling problem for a general FAS-assisted UAV-to-GU channel. The model can characterize the channel features of FAS in diverse scenarios, thereby exploring the feasibility and performance potential of FAS in practical applications from the perspective of channel modeling. Through theoretical analysis and simulation validation, the accuracy and channel capacity of the proposed

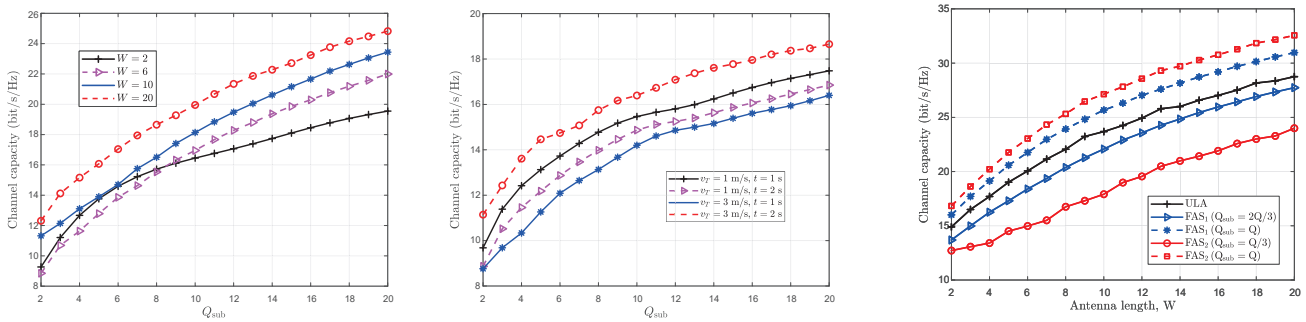

(a) Capacity of the proposed FAS with different sizes.

(b) Capacity of the proposed FAS with different motion states.

(c) Channel capacity of the proposed FAS and ULA, where $\text{FAS}_1 : \Delta d = \lambda/3$ and $\text{FAS}_2 : \Delta d = \lambda/4$.

Fig. 5. Performance analysis of the proposed FAS channel model.

model have been studied. It has been demonstrated that the number of active ports and the spacing between ports significantly impact both the model accuracy and channel capacity. Specifically, more active ports will bring high channel capacity but high modeling error. Moreover, the dynamic characteristics of UAVs, such as their velocities and motion time, also play a crucial role in determining the channel capacity. Finally, it should be pointed out that detailed research on Doppler phase shift is a key research direction in our future research.

REFERENCES

[1] F. Tariq *et al.*, "A speculative study on 6G," *IEEE Wireless Commun.*, vol. 27, no. 4, pp. 118–125, Aug. 2020.

[2] G. Gui, M. Liu, F. Tang, N. Kato and F. Adachi, "6G: Opening new horizons for integration of comfort, security, and intelligence," *IEEE Wireless Commun.*, vol. 27, no. 5, pp. 126–132, Oct. 2020.

[3] H. Yu, T. Taleb, K. Samdanis and J. Song, "Toward supporting holographic services over deterministic 6G integrated terrestrial and non-terrestrial networks," *IEEE Netw.*, vol. 38, no. 1, pp. 262–271, Jan. 2024.

[4] E. G. Larsson, O. Edfors, F. Tufvesson and T. L. Marzetta, "Massive MIMO for next generation wireless systems," *IEEE Commun. Mag.*, vol. 52, no. 2, pp. 186–195, Feb. 2014.

[5] C. Ruan *et al.*, "Simplified learned approximate message passing network for beamspace channel estimation in mmWave massive MIMO systems," *IEEE Trans. Wireless Commun.*, vol. 23, no. 5, pp. 5142–5156, May 2024.

[6] H. Jiang *et al.*, "High-Efficient Near-Field Channel characteristics analysis for large-scale MIMO communication systems," *IEEE Internet Things J.*, vol. 12, no. 6, pp. 7446-7458, Mar. 2025.

[7] W. K. New *et al.*, "A tutorial on fluid antenna system for 6G networks: Encompassing communication theory, optimization methods and hardware designs," *IEEE Commun. Surv. & Tutor.*, doi:10.1109/COMST.2024.3498855, 2024.

[8] K. K. Wong, K. F. Tong, Y. Zhang, and Z. Zheng, "Fluid antenna system for 6G: When Bruce Lee inspires wireless communications," *IET Elect. Lett.*, vol. 56, no. 24, pp. 1288–1290, Nov. 2020.

[9] K. K. Wong, A. Shojaeifard, K. F. Tong, and Y. Zhang, "Performance limits of fluid antenna systems," *IEEE Commun. Lett.*, vol. 24, no. 11, pp. 2469–2472, Nov. 2020.

[10] K. K. Wong, A. Shojaeifard, K. F. Tong, and Y. Zhang, "Fluid antenna systems," *IEEE Trans. Wireless Commun.*, vol. 20, no. 3, pp. 1950–1962, Mar. 2021.

[11] W.-J. Lu *et al.*, "Fluid antennas: Reshaping intrinsic properties for flexible radiation characteristics in intelligent wireless networks," accepted in *IEEE Commun. Mag.*, 2025.

[12] Y. Shen *et al.*, "Design and implementation of mmWave surface wave enabled fluid antennas and experimental results for fluid antenna multiple access," *arXiv preprint*, arXiv:2405.09663, May 2024.

[13] M. Khammassi, A. Kammoun, and M.-S. Alouini, "A new analytical approximation of the fluid antenna system channel," *IEEE Trans. Wireless Commun.*, vol. 22, no. 12, pp. 8843–8858, Dec. 2023.

[14] P. Ramírez-Espinosa, D. Morales-Jimenez, and K. K. Wong, "A new spatial block-correlation model for fluid antenna systems," *IEEE Trans. Wireless Commun.*, vol. 23, no. 11, pp. 15829–15843, Nov. 2024.

[15] P. D. Alvim *et al.*, "On the performance of fluid antennas systems under α-μ fading channels," *IEEE Wireless Commun. Lett.*, vol. 13, no. 1, pp. 108–112, Jan. 2024.

[16] W. K. New, K. K. Wong, H. Xu, K. F. Tong and C.-B. Chae, "Fluid antenna system: New insights on outage probability and diversity gain," *IEEE Trans. Wireless Commun.*, vol. 23, no. 1, pp. 128–140, Jan. 2024.

[17] W. K. New, K. K. Wong, H. Xu, K. F. Tong, and C.-B. Chae, "An information-theoretic characterization of MIMO-FAS: Optimization, diversity-multiplexing tradeoff and q-outage capacity," *IEEE Trans. Wireless Commun.*, vol. 23, no. 6, pp. 5541–5556, Jun. 2024.

[18] C. Psomas, P. J. Smith, H. A. Suraweera, and I. Krikidis, "Continuous fluid antenna systems: Modeling and analysis," *IEEE Commun. Lett.*, vol. 27, no. 12, pp. 3370–3374, Dec. 2023.

[19] K. K. Wong and K. F. Tong, "Fluid antenna multiple access," *IEEE Trans. Wireless Commun.*, vol. 21, no. 7, pp. 4801–4815, Jul. 2022.

[20] K. K. Wong, K. F. Tong, Y. Chen, and Y. Zhang, "Fast fluid antenna multiple access enabling massive connectivity," *IEEE Commun. Lett.*, vol. 27, no. 2, pp. 711–715, Feb. 2023.

[21] K. K. Wong, D. Morales-Jimenez, K. F. Tong, and C.-B. Chae, "Slow fluid antenna multiple access," *IEEE Trans. Commun.*, vol. 71, no. 5, pp. 2831–2846, May 2023.

[22] K. K. Wong, C.-B. Chae, and K. F. Tong, "Compact ultra massive antenna array: A simple open-loop massive connectivity scheme," *IEEE Trans. Wireless Commun.*, vol. 23, no. 6, pp. 6279–6294, Jun. 2024.

[23] H. Hong, K. K. Wong, K. F. Tong, H. Shin, and Y. Zhang, "Coded fluid antenna multiple access over fast fading channels," accepted in *IEEE Wireless Commun. Lett.*, 2025.

[24] S. B. S. Abdou *et al.*, "Sum-Rate Maximization for UAV Relay-Aided Fluid Antenna System with NOMA," in *Proc. 2024 IEEE 7th International Symposium on Telecommunication Technologies (ISTT)*, Langkawi Island, Malaysia, 2024.

[25] Ghadi, F. R. *et al.*, "UAV-Relay Assisted RSMA Fluid Antenna System: Outage Probability Analysis." *arXiv preprint* arXiv:2503.16751, 2025.

[26] N. Waqar *et al.*, "Opportunistic fluid antenna multiple access via team-inspired reinforcement learning," *IEEE Trans. Wireless Commun.*, vol. 23, no. 9, pp. 12068–12083, Sept. 2024.

[27] H. Xu *et al.*, "Channel estimation for FAS-assisted multi-user mmWave systems," *IEEE Commun. Lett.*, vol. 28, no. 3, pp. 632–636, Mar. 2024.

[28] W. K. New *et al.*, "Channel estimation and reconstruction in fluid antenna system: Oversampling is essential," *IEEE Trans. Wireless Commun.*, vol. 24, no. 1, pp. 309–322, Jan. 2025.

[29] F. R. Ghadi *et al.*, "On performance of RIS-aided fluid antenna systems," *IEEE Wireless Commun. Lett.*, vol. 13, no. 8, pp. 2175–2179, Aug. 2024.

[30] X. Lai *et al.*, "FAS-RIS: A block-correlation model analysis," *IEEE Trans. Veh. Technol.*, vol. 74, no. 2, pp. 3412–3417, Feb. 2025.

[31] H. Jiang *et al.*, "Large-scale RIS enabled air-ground channels: near-field modeling and analysis," *IEEE Trans. Wireless Commun.*, vol. 24, no. 2, pp. 1074-1088, Feb. 2025

[32] R. Feng *et al.*, "Classification and comparison of massive MIMO propagation channel models," *IEEE Internet Things J.*, vol. 9, no. 23, pp. 23452-23471, Dec. 2022.